



Constructing an 8 element RF Coil Array for a Portable, Low-cost MRI Scanner

THESIS

submitted in partial fulfillment of the
requirements for the degree of

BACHELOR OF SCIENCE

in

PHYSICS

Author :	Jaimy Plugge
Student ID :	1654845
Supervisor :	Prof. Dr. Andrew G. Webb
2 nd corrector :	Prof. Dr. Ir. Tjerk H. Oosterkamp

Leiden, The Netherlands, July 10, 2018

Constructing an 8 element RF Coil Array for a Portable, Low-cost MRI Scanner

Jaimy Plugge

Huygens-Kamerlingh Onnes Laboratory, Leiden University
P.O. Box 9500, 2300 RA Leiden, The Netherlands

July 10, 2018

Abstract

Low-Field MRI systems without gradients have problems with spatial encoding and low SNR due to the low magnetic field (B_0). In this project, an 8 element RF coil array is constructed for extra spatial encoding. This thesis describes the idea of Low-Field MRI, how 2D images can be constructed inside its field, the construction of coils and how these coils must be tuned and matched.

Contents

1	Introduction	7
2	Theory	9
2.1	Magnetic Resonance Imaging	9
2.2	Low-Field MRI	10
2.3	LC-circuits	13
2.4	Multiple windings	14
2.5	Tuning and impedance matching	16
2.6	Sensitivity Encoding	19
2.7	Coupling	21
2.8	Inhomogeneity of the Magnetic Field	24
2.9	Spin Echo	26
3	Methodology	27
3.1	Coils	27
3.2	2D images	27
4	Results	31
4.1	First measurements	31
4.2	2D images	32
4.3	Sensitivity Encoding	36
5	Discussion	43
6	Conclusion	45
6.1	Acknowledgements	45

Chapter 1

Introduction

In sub-Saharan Africa, the amount of new cases of hydrocephalus in infants exceeds 200 000 every year [1]. Hydrocephalus is a condition in which patients suffer from an accumulation of cerebrospinal fluid (CSF) which can easily be diagnosed with MRI (Magnetic Resonance Imaging). The problem, however, is that a lot of patients in sub-Saharan Africa do not have the opportunity to go to a hospital with a MRI machine. As reported by the World Health Organization (WHO), Uganda (the country we focused on) only has 3 MRI scanners which equates to about 0.08 scanners per million inhabitants [2]. A great way to overcome this problem would be to use low-cost MRI systems that are portable to be able to get them to remote areas.

MRI systems map the location of water (among other hydrogen containing molecules) inside the body, which makes them useful for the examination of hydrocephalus. The advantages of MRI include high quality images, no use of ionizing radiation, 2D and 3D images from multiple angles and being able to distinguish between body parts. A big disadvantage however, is that MRI requires a strong homogeneous magnetic field which is obtained from superconducting wires. For these wires to be superconducting, they are kept at 4.2K inside a Cryostat filled with liquid Helium. A lot of bulk has to be added to the system to avoid the helium (and eventually the wires) from heating up.

This bulk is what held people back from developing portable MRIs. Because to create a portable MRI scanner, the standard concept of MRI has to be reconsidered. Instead of a big superconducting magnet, we want our magnetic field to come from permanent magnets. Those permanent magnets, however, produce a weak and inhomogeneous field. The challenge of obtaining a signal from these magnets is that the signal from MR is pro-

portional to B_0^2 . Since our magnetic field is about 25 times lower than the field of conventional MRI scanners (1.5T), this equates to about 625 times less signal.

Because of the low magnitude of our signal, the RF (radio frequency) coils have to be very sensitive to measure some signal with a high signal-to-noise ratio (SNR). Inspired by Cooley et al [3], we will use multiple transmit and receive RF coils to measure our MR signal. This also gives us the opportunity to use them to get spatial information. For that, each of the coils gets sequentially excited and from that we will be able to construct a 2D image from the sample inside the magnet. These coils need to have a center frequency of 2.5 MHz since that is the Larmor frequency for protons inside a magnetic field of 58 mT.

The question is if it is possible to construct a high resolution 2D image from the 8 coils that will be designed by us. To answer this question, we first have to take a look at the process of designing a coil. Then we have to make sure the multiple coils don't couple, so we have to find a way to minimize the coupling effect. Additionally, we want to use our B_0 homogeneity for extra spatial encoding.

Theory

2.1 Magnetic Resonance Imaging

Every atom is, next to electrons and often neutrons, made out of protons. Those protons can be seen as small magnets which want to align with a magnetic field (B_0) when one is present (as shown in figure 2.1).

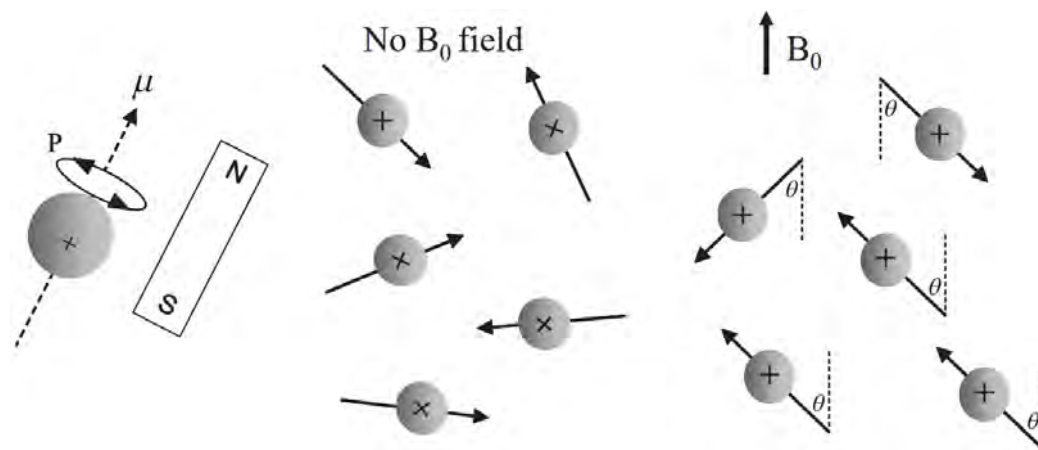


Figure 2.1: [4] Protons with magnetic moment μ and angular moment P .

MRI is based on the concept of measuring this proton alignment, especially those in hydrogen nuclei (which contain one proton per atom). After these protons are aligned to B_0 (in the Z-direction), a short RF pulse (B_1) which is orthogonal to B_0 excites these protons and creates torque. This causes them to align their net magnetization in the XY-plane in which they start to rotate as can be seen in figure 2.2.

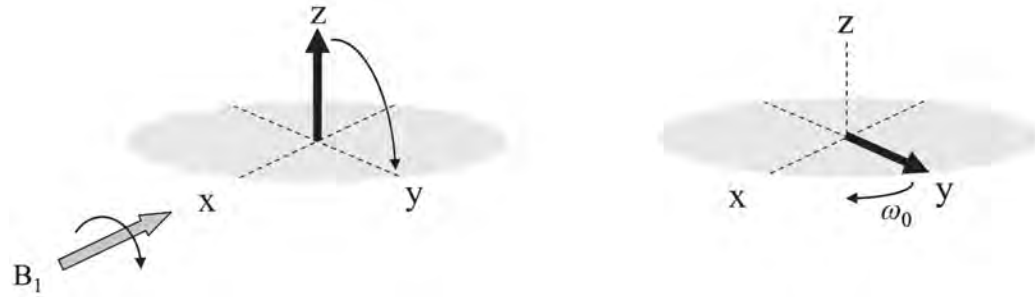


Figure 2.2: [4] B_1 field rotates the net magnetization to the XY-plane.

After the RF pulse gets turned off, the spins want to realign with the B_0 -field following the formula:

$$M_Z = M_0 e^{-\frac{t}{T_1}} \quad (2.1)$$

Every type of material has a different T_1 , which is (among other ways) used to differentiate between material types in MRI. The spacial encoding is done by applying a gradient in the magnetic field in multiple directions.

As described by Smith and Webb in [4], the strength of the MR signal is proportional to the following factors: The number of protons in the sample, the net magnetization of the sample and the induced voltage. The net magnetization is given by:

$$M_0 = \frac{\gamma^2 h^2 B_0 N_{Total}}{16\pi^2 k_b T} \quad (2.2)$$

The magnitude of the induced voltage is proportional to the frequency in which the proton precesses, which is given by:

$$\begin{aligned} \omega &= \gamma B_0 \\ V_0 &= -\frac{\partial B}{\partial t} \propto M_0 \omega \propto B_0^2 \end{aligned} \quad (2.3)$$

This means that in total, the signal is proportional to B_0^2 , which gives the reason conventional MRI is done at a high magnetic field.

2.2 Low-Field MRI

The B_0 -field has to be very homogeneous to construct clear images, in conventional MRI this is done with a strong electromagnet. The problem with

electromagnets, however, is that they need to be powered which results in extra bulk. As already demonstrated by Cooley et al [3], it is also possible to obtain an homogeneous magnetic field from an Halbach magnet array [5]. Halbach magnet arrays are constructed by positioning permanent magnets in a specific way to create a high magnetic field at one side of the array and a lower field at the other side (figure 2.3).

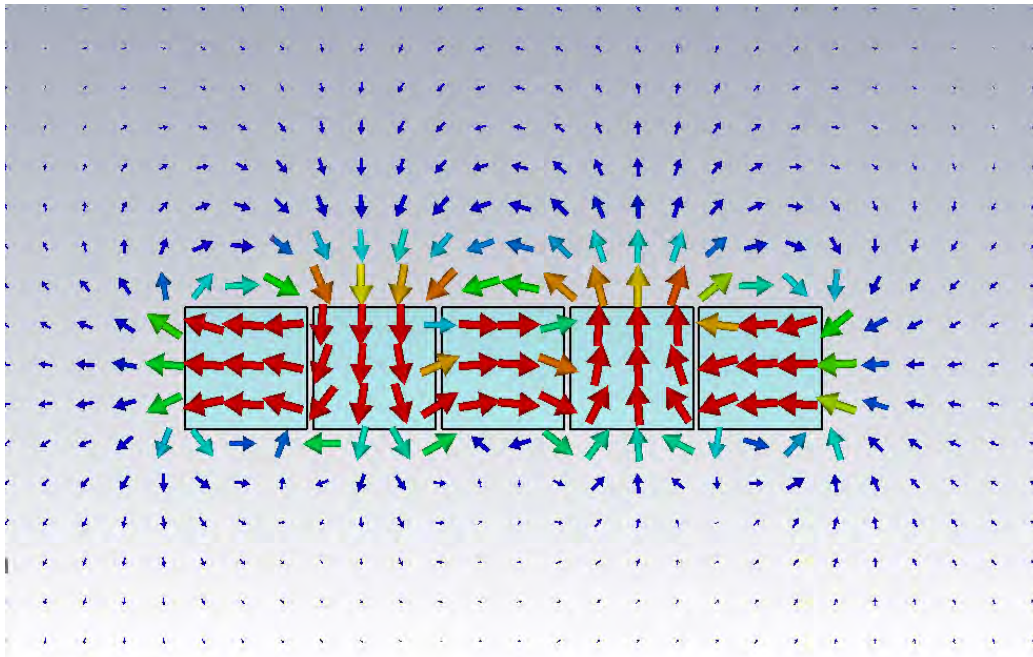


Figure 2.3: Simulation of the magnetic field of an Halbach array, the red arrows show the direction of the magnetic field inside each magnet. Red and bigger arrows correspond to higher magnetic field strengths, blue and small to lower field strengths.

Simulation data provided by Thomas O'Reilly.

As described by Blümler and Casanova [6], when placed in a ring (figure 2.4), these arrays form a circle in which the magnetic field aims in the same direction. In theory, this would result in a homogeneous magnetic field inside the whole circle. That is, however, only if we had an infinite tube of magnets with a continuous change in magnetic field direction through the walls of the ring (figure 2.4a versus 2.4b). Since it is for us not possible to create a ring which consists of a wall with a continuously changing magnetic field direction inside, we had to construct the discrete case. Figure 2.5a shows a schematic design of the Halbach ring TU Delft DEMO (Electronic and Mechanical Support Division) constructed of which the magnetic field is simulated in figure 2.5b.

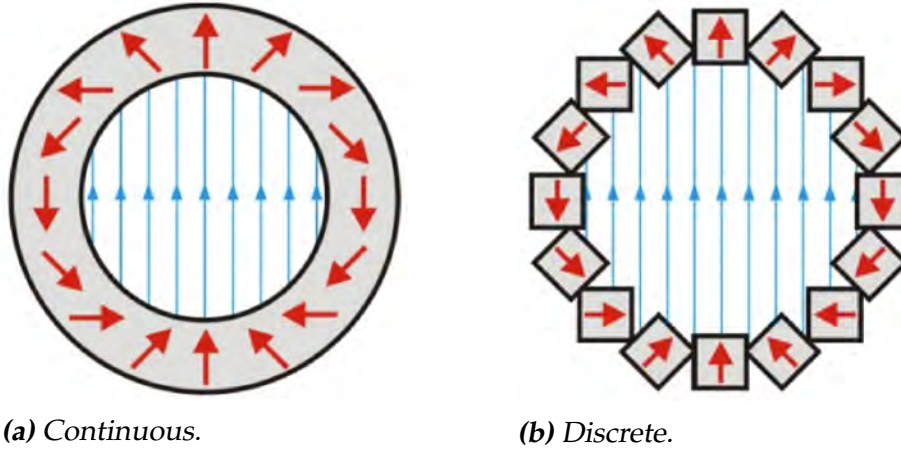


Figure 2.4: [6] Designs of a Halbach Ring.

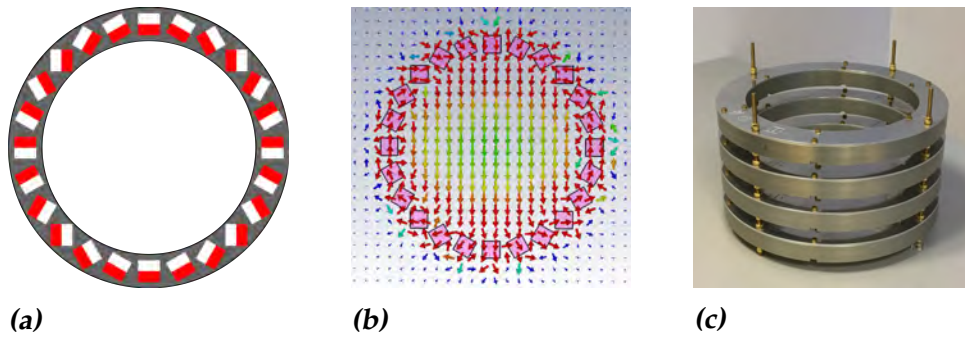


Figure 2.5: The orientation of the magnets inside the rings is shown in (a), red is north. (b) Is a simulation of the field lines inside one of the rings shown in (c).

Simulation data provided by Thomas O'Reilly.

As shown in equation 2.3, the frequency in which the proton processes depends linearly on the magnetic field strength. The frequency of the RF pulse (B_1^+) used to flip the protons to the XY-plane follows the same relation. Our magnetic field $B_0 \approx 58mT$ and since the gyromagnetic ratio (γ) of a proton is given by $2.68 \cdot 10^8 s^{-1} T^{-1}$, this gives for our RF pulse:

$$1.6 \cdot 10^6 \text{rads}^{-1} \approx 2.5 \text{MHz} \quad (2.4)$$

This is the reason the coils made for this project have to operate at center frequency 2.5 MHz. But as can be seen in figure 2.6a, the magnetic field is not perfectly homogeneous. A problem with an inhomogeneous field is that a single RF coil can only excite a limited range of frequencies at the same time which results in a small field of view for the coils which will be further explained in chapter 2.8.

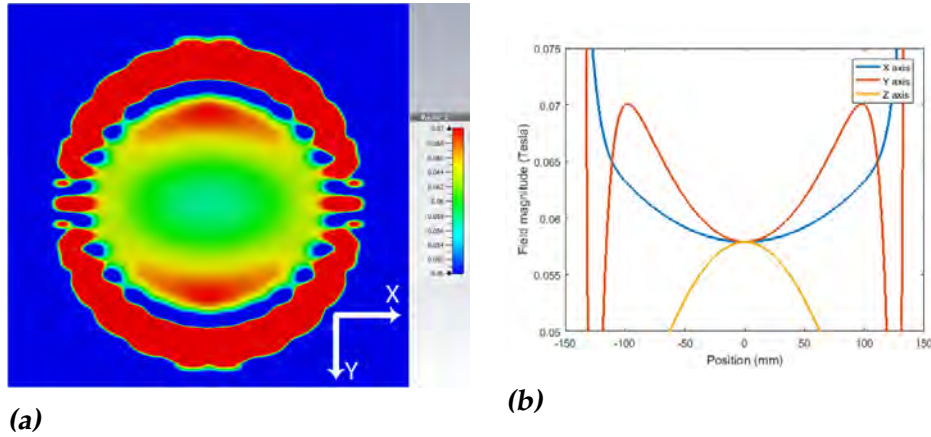


Figure 2.6: (a) is simulation of the magnetic field inside the magnet, the scale is in T. In (b), a graph of the field strength as a function of the position is shown.

Simulation data provided by Thomas O'Reilly.

2.3 LC-circuits

A LC-circuit is an harmonic oscillator which stores its energy at its resonance frequency, this can be seen by looking at a standard LC-circuit (figure 2.7). Following Kirchhoff's voltage law, the sum of the voltages over the inductor and the capacitor must be equal to 0. Also, the current through the inductor and the capacitor must be the same according to Kirchhoff's current law:

$$\begin{aligned} V_C + V_L &= 0 \\ I_C &= I_L := I \end{aligned} \quad (2.5)$$

This leads to the following equation:

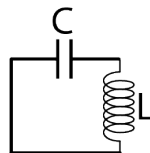


Figure 2.7: Standard LC-circuit

$$\begin{aligned}
V_L &= L \frac{dI_L}{dt} \\
&= L \frac{dI}{dt} \\
I_C &= C \frac{dV_C}{dt} \\
&= C \frac{d(-V_L)}{dt} \\
&= -LC \frac{d}{dt} \left(\frac{dI}{dt} \right) \\
&= -LC \frac{d^2 I}{dt^2} = I
\end{aligned} \tag{2.6}$$

From which we obtain the differential equation:

$$\frac{d^2 I}{dt^2} = -\frac{1}{LC} I(t) \tag{2.7}$$

This differential equation can be compared to the differential equation of an harmonic oscillator:

$$\frac{d^2 f}{dt^2} = -\omega^2 f(t) \tag{2.8}$$

With ω being the resonance frequency of the harmonic oscillator. This gives for the resonance frequency of the LC-circuit:

$$\omega_{resonance} = \sqrt{\frac{1}{LC}} \tag{2.9}$$

2.4 Multiple windings

The first coils made especially for the eight-coil array were made out of flexible PCBs (Printable Circuit Board) (figure 3.1c). The problem with this coil was that it was made out of a single winding, which resulted in a lower inductance than we wanted to have. As shown in equation 2.9, the resonance frequency depends on the inductance of the coil and the capacitance of the tuning coil. Since we know our resonance frequency, we can rewrite equation 2.9 as:

$$\begin{aligned}
\omega_R &= \frac{1}{\sqrt{LC}} \\
2\pi f_R &= \frac{1}{\sqrt{LC}} \\
4\pi^2 f_R^2 &= \frac{1}{LC} \\
\frac{1}{4\pi^2 f_R^2} &= LC \\
LC &\approx 4.05 \cdot 10^{-15} \text{ HF}
\end{aligned} \tag{2.10}$$

This equations shows that the lower the inductance, the higher the capacitance of the tuning capacitor needs to be. However, capacitors with higher capacitor values tend to have more losses. To be able to use lower capacitance, our coils need a higher inductance. The inductance of a coil follows the following equation:

$$L = \frac{\mu_0 N^2 A}{l} = \mu_0 n N A$$

With:

$$\begin{aligned}
\mu_0 &= \text{The magnetic constant} \\
N &= \text{The number of windings} \\
A &= \text{The area of the coil} \\
l &= \text{The length of the coil} \\
n &= \text{The amount of windings per unit length}
\end{aligned} \tag{2.11}$$

Here it can be seen that the inductance will increase with the amount of turns of the coil. So eventually, more windings means lower capacitor values can be used. More windings, however, will eventually make the self inductance of the coil a bigger problem. The self-inductance is caused by energy of the coil stored in the magnetic field and linearly depends on the inductance of the coil. For this reason, we eventually chose for coils with 8 turns (3.1d), because calculated from equation 2.10 they had an inductance of about $334\mu H$ (compared to an inductance of $7.6\mu H$ for the coil with a single winding). This requires tuning capacitors in the range of hundreds pF instead of tens nF.

The capacitor value also has an effect on the Q-factor. The Q-factor is a parameter that describes the amount of energy loss in an harmonic

oscillator. A higher Q-factor means that the system has less energy loss per cycle than a system with a low Q-factor. A LC-circuit acts like a harmonic oscillator for current that stores its energy at its resonance frequency. This means that a LC-circuit also has a Q-factor which is inverse dependent on the bandwidth around the resonance frequency of the energy stored in the magnetic field.

2.5 Tuning and impedance matching

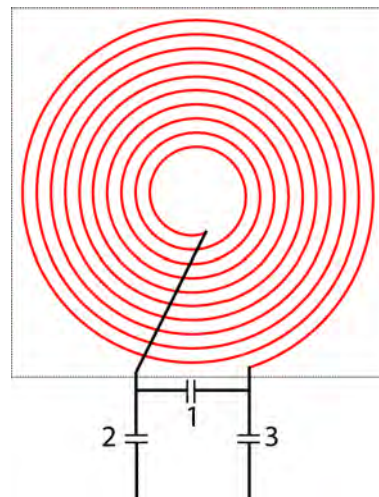


Figure 2.8: Scheme of the Coil (inside dotted square), the tuning capacitor (1) and the matching capacitors (2 and 3). The spiral has an inner diameter of 3 mm and an outer diameter of 85 mm. Note that this scheme is made to have a schematic idea of the coil, the real coil has no space between the wires and has 17 windings

The coils need to induce a B_1 -field at 2.5 MHz, which can be done by adding capacitors to the circuit. Figure 2.8 shows a scheme of the spiral coil with the capacitors. Here we distinguish between *tuning* and *matching* coils. The tuning capacitor changes the resonance frequency of the coil, since we can approximate the circuit by a standard LC-circuit for which we know that:

$$\omega_{resonance} = \frac{1}{\sqrt{LC}} \quad (2.12)$$

The inductor is already made and cannot be changed without redesigning the coil. This means the only way to change the resonance frequency is by varying the tuning capacitor. A consequence is that, according to equation

2.12, for ω_R to be $\frac{2}{3}$ times smaller, C_{tuning} has to approximately be $\frac{9}{4}$ times bigger.

After one found the resonance frequency, the system (coil + tuning capacitor) has to be impedance matched to the network. When an RF signal transitions from one medium to another, similar to light, reflections can occur. Let every element of \vec{a} be every incoming signal and the elements of \vec{b} the reflected signal, then those signals and the scattering parameter (S-parameter) have the following relation:

$$\vec{b} = \mathbf{S}\vec{a}$$

$$\begin{pmatrix} b_1 \\ b_2 \end{pmatrix} = \begin{pmatrix} S_{11} & S_{12} \\ S_{21} & S_{22} \end{pmatrix} \begin{pmatrix} a_1 \\ a_2 \end{pmatrix} \quad (2.13)$$

Here, $\mathbf{S} = 0$ corresponds to zero reflection, which can also be seen in the formula of the S_{11} -parameter in terms of the impedance:

$$S_{11}(\omega) = \frac{Z(\omega) - Z_0}{Z(\omega) + Z_0} \quad (2.14)$$

With Z_0 the reference impedance, so when $Z(\omega) = Z_0$, $S(\omega) = 0$. Since impedance of the electronics in MR are designed to be 50Ω , we want the impedance of our coils to be 50Ω too:

$$S(\omega) = \frac{Z(\omega) - 50\Omega}{Z(\omega) + 50\Omega} \quad (2.15)$$

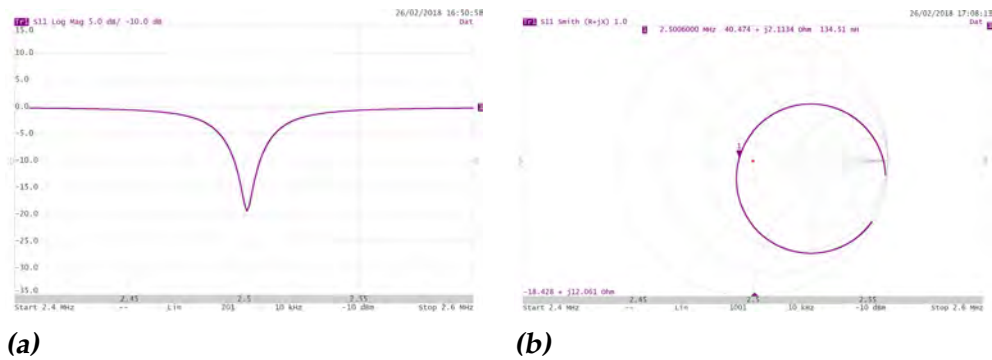


Figure 2.9: Screenshots of the network analyzer with the spiral coil attached, (a) is a S_{11} Logarithmic Magnitude (Log Mag) plot and (b) a Smith chart, the red dot is at $50 + 0j \Omega$.

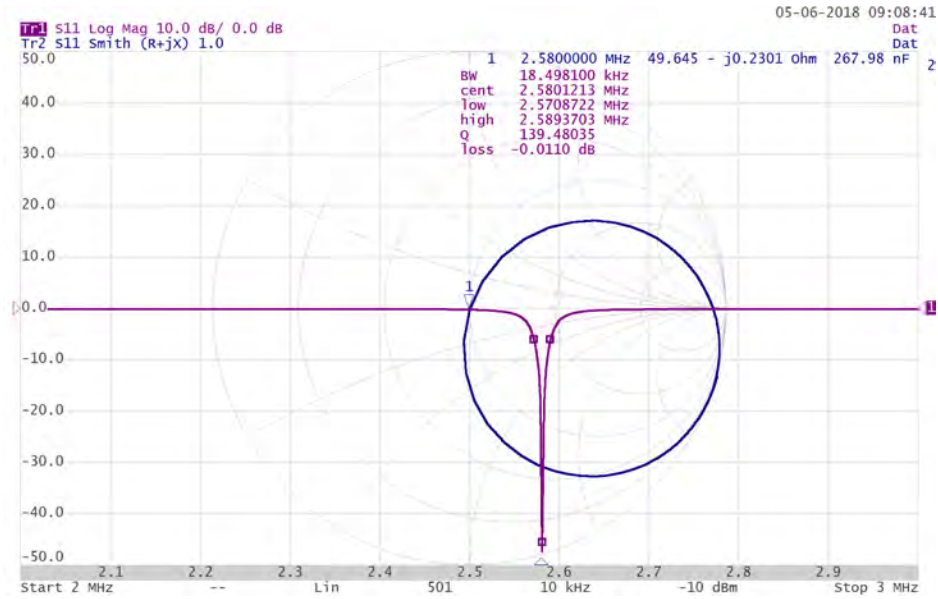


Figure 2.10: A smith chart and a Log Mag plot of an almost ideally tuned and matched coil.

To check if the coil is tuned and matched as desired, the system is connected via a coaxial cable (under C_2 and C_3 in figure 2.8) to a network analyzer* to perform a S_{11} measurement. As can be seen in figure 2.9a, the network analyzer plots the frequencies (in MHz) versus the amount of reflection (in decibel) following:

$$S(f, dB) = 20 \log_{10}(S(f)) \quad (2.16)$$

The deeper the peak in the Log Mag plot (Logarithmic Magnitude), the better the system is matched with the network. To understand how the matching capacitors have to be changed, a Smith chart (Figure 2.9b) is used. In a Smith chart, the ideal coil has its resonance frequency at $50 + 0j \Omega$ (the middle of the Smith chart).

The impedance of the resonance frequency of the coil can be brought to $50 + 0j \Omega$ by changing the matching capacitors. As shown in figure 2.10, the blue line has a circular shape. By varying the capacity of the matching capacitors (while keeping both of them somewhat the same value), the circle changes in diameter. The bigger the capacitance, the bigger the circle gets. The tuning capacitor rotates the circle around its centre, by increasing its capacitance the circle rotates to the left.

*The network analyzer we used is a "Planar TR1300/1" from Copper Mountain Technologies

The difference matching makes can be seen by comparing figure 2.9a and 2.10.

2.6 Sensitivity Encoding

In conventional MRI systems, receive coil sensitivity encoding is used to reduce the scanning time. By using multiple coils around the sample of which the sensitivity maps are known, fewer points in k-space have to be sampled while still obtaining the same image [7]. But since we do not sample our points in k-space, we use our coil sensitivity in a different way. Figure 2.11 shows a schematic overview of our procedure.

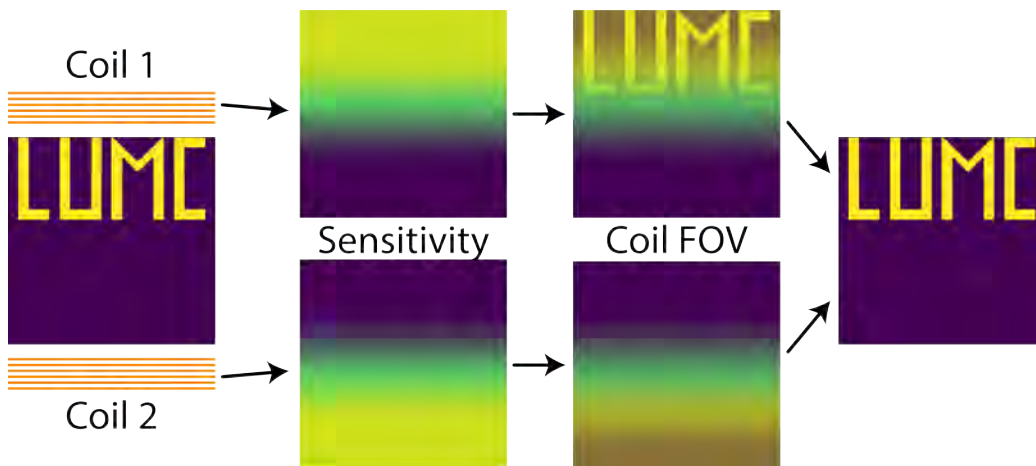


Figure 2.11: Schematic view of Sensitivity encoding with the LUMC phantom, only coil 1 is able to see the full phantom, coil 2 can only see a small part of the bottom.

As shown in this figure, coil 1 ‘sees’ more of the phantom than the other one. This means that coil 1 will obtain more signal from this phantom than coil 2. Since we know the location of our coils, we can reconstruct the image of the phantom with the help of the sensitivity maps of the coils. This technique can also be used for extra spatial encoding, which is beneficial for this project. The difference, however, is that the math for this technique in conventional MRI systems differs from the math in our project since we do not have a linear gradient in our field like conventional systems do.

The model of the signal acquired in our measurements of a single coil is given by [3]:

$$s_{q,r}(t) = \sum_{\vec{x}} C_{q,r}(\vec{x}) e^{-i2\pi k(r,\vec{x},t)} m(\vec{x}) \quad (2.17)$$

In this equation, q is the coiled used for the measurement and r the specific rotation of the magnetic field at time t . The magnetization of the sample at a position \vec{x} is given by $m(\vec{x})$, so $m(\vec{x})$ is what we want to obtain. $C_{q,r}$ contains information of the sensitivity of a coil q , at rotation r and position \vec{x} . $C_{q,r}$ depends on the rotations since the coil sensitivity depends on the vector perpendicular to the B_0 -field. Without $C_{q,r}$, the symmetry in the reconstruction (which will be further explained in chapter 3.2) would still be present. The phase of the protons in our magnetic field is described by k . When written in matrix form it is convenient to merge both C and k in an encoding matrix $\mathbf{E}_{q,r}$:

$$\vec{S}_{q,r} = \mathbf{E}_{q,r} \vec{m} \quad (2.18)$$

Since we want to solve for \vec{m} and we know $\vec{S}_{q,r}$ and $\mathbf{E}_{q,r}$, we have to invert the matrix $\mathbf{E}_{q,r}$. The problem here is that $\mathbf{E}_{q,r}$ is a large matrix ($N_{\text{samplepoints}} \cdot N_{\text{rotations}} \cdot N_{\text{coils}} \times N_{\text{voxels}}$) which cannot easily be inverted. This is then solved by iteratively changing \vec{m} until equation 2.18 is as close to being true as possible.

In figure 2.12, some simulations of sensitivity encoding on the LUMC phantom in our magnetic field are shown.

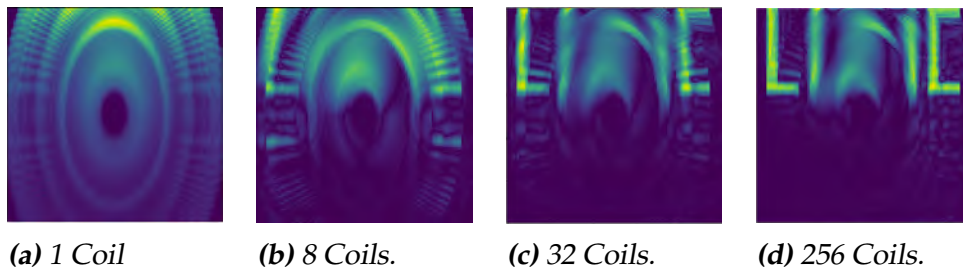


Figure 2.12: Reconstruction of the LUMC phantom only by sensitivity encoding. Different amounts of coils are placed evenly in a circle around the sample with their normal vector perpendicular to the circumference of that circle. Except for (a), that one is made by one coil with an even sensitivity over the whole sample.

Simulation data provided by Thomas O'Reilly.

2.7 Coupling

When multiple coils with close to the same resonance frequency are close to each other, energy from one of them will end up in the other. This is what we call coupling of the coils. We do not want our coils to couple with each other because we want as much energy as possible to go into the sample. As explained in chapter 2.3, a LC-circuit is an harmonic oscillator. This means that two coupled LC-circuits can be compared to coupled pendula[8] (figure 2.13a) which are coupled by a spring with spring constant k . This coupled pendulum has two normal modes, in the first mode both pendula oscillate in phase which means the spring does not exert any force on the pendula. Since the spring does not play a role in this normal mode, it can be replaced by something without a spring constant (figure 2.13b). In the other normal mode, the pendula oscillate in anti-phase (figure 2.13c). Here it can be seen that the middle of the spring stays fixed, which means that the spring can be replaced by two springs with spring constant $2k$ that are connected to a fixed point in the middle of the pendula (figure 2.13d).

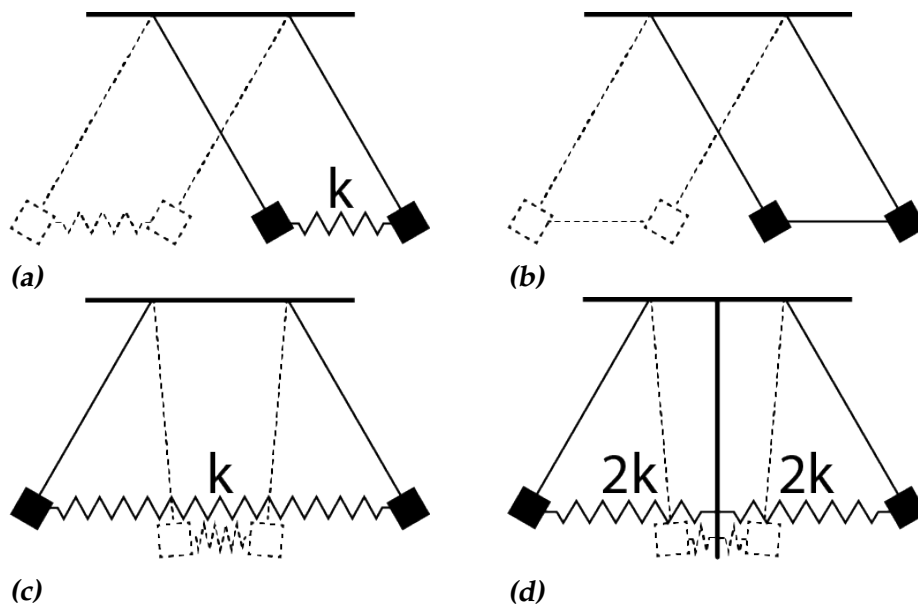


Figure 2.13

When two LC-circuits are close to each other they can couple through induction, this coupling is called M in figure 2.14a. This inductive coupling can for both LC-circuits be replaced by a coil with induction M , but

then we have to add a coil to both circuits with induction $L - M$ (figure 2.14b). From here on, we use what we know from the coupled pendula: The circuits should have two normal modes, one where they oscillate in phase and the other where the circuits oscillate in anti-phase. With in-phase oscillation, no current flows through M , so it can be taken out of the circuit (comparable to in-phase oscillation of the harmonic oscillator) (figure 2.14c). But now, for both LC-circuits, the resonance frequency is shifted since we do not have an inductance L , but $L - M$. For anti-phase oscillation, twice the current flows through M , so equally to the spring being replaced by two springs with double the spring constant, the inductor M can be replaced by two inductors with inductance $2M$ (figure 2.14d). In series, impedances of components can be added, so we can now replace the two inductors by one inductor with an inductance of $L + M$ which means this resonance frequency is also shifted. This gives for our resonance frequencies:

$$\omega_{\pm} = \sqrt{\frac{1}{(L \mp M)C}} \quad (2.19)$$

With ω_+ the resonance frequency for in-phase motion and ω_- for anti-phase motion. This means the resonance frequency of the the LC-circuit without coupling is shifted by:

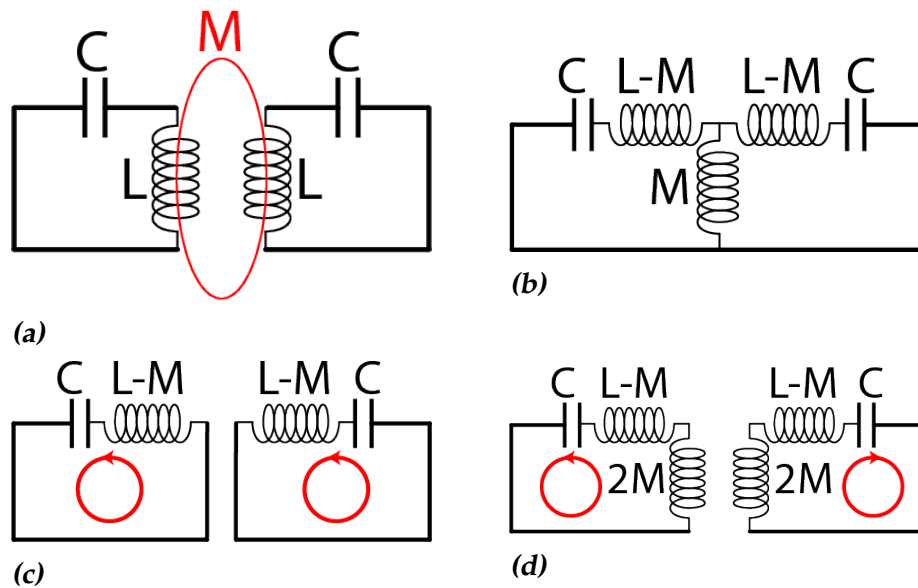
$$\omega_{\pm} = \omega_o \sqrt{\frac{1}{1 \mp k}} \quad (2.20)$$

With the coupling constant k equal to $\frac{M}{L}$ [9].

So not only will some of our energy end up in the coupled coil, but our coil will also have two other resonance frequencies in which it oscillates instead of the resonance frequency we want it to have. A solution to 'decouple' your coils is by overlapping them, this is called geometric decoupling. The reason this works is shown in figure 2.15. When two coils are brought closer to each other, they will eventually overlap so much that the magnetic field in one direction cancels the magnetic field in the other direction which means no induction in the coupled coil.

To measure this coupling, a S_{21} -measurement (see equation 2.13) has to be done with the network analyzer[†]. With an S_{21} measurement, the amount of signal that comes from port 2 gets measured at port 1. We want that signal to be as low as possible. We were able to decouple every

[†]The network analyzer we used is a "Planar TR1300/1" from Copper Mountain Technologies

**Figure 2.14**

coil with their direct neighbour, the problem came however with the next nearest neighbour. Since it is impossible to decouple them geometrically, we had to hope their coupling was minimal. However, their coupling was so big, they still had their resonance peaks split (figure 2.16a vs 2.16b). Because of this, we will not be able to measure with every coil of the coil array at the same time. It may in theory be possible to measure with two coils at the same time which would mean we only have to detune 6 coils, but we do not have the hardware to transceive with multiple coils at the same time. So we have to detune the other seven coils while we are using one of the coils for a measurement. This is a big disadvantage because it increases the scanning time by a factor 8. To detune the coils, a switch is added to the circuit to prevent current from going through the coils.

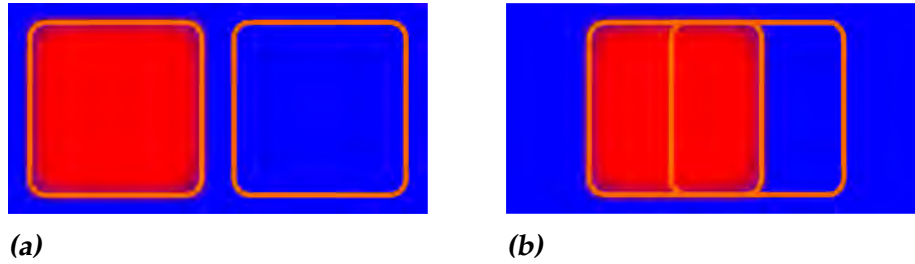


Figure 2.15: 2 Coils (in orange) with a rough sketch of the direction of the field lines produced by the left coil. Blue and red point in opposite directions. (a) shows two coils close to each other, the magnetic field produced by the left coil goes through the right coil; they are coupled. In (b), the magnetic field inside the right coil coming from the left coil cancels out because an equal amount of red and blue are inside the right coil; they are geometrically decoupled.

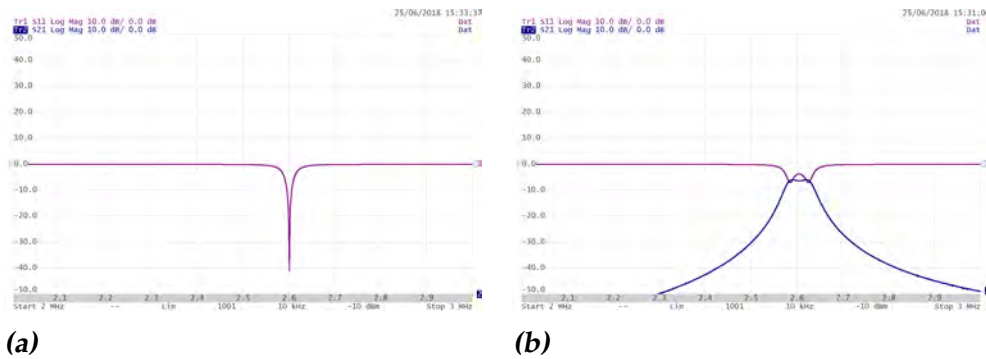


Figure 2.16: Screenshots of a S_{11} (purple) and a S_{12} (blue) Log Mag plot of a coil and its next nearest neighbor with one coil tuned and the rest detuned (a) and with both coils tuned (b).

2.8 Inhomogeneity of the Magnetic Field

In inhomogeneous fields, coils can excite a smaller volume than coils with the same bandwidth in a homogeneous field. The broader the bandwidth, the more field strengths can be excited by that coil. But at some point, a field is so inhomogeneous that the bandwidth of the coil can practically be not broad enough to excite the whole volume of that field. Figure 2.17a shows the B_0 -field map of a $10\text{ cm} \times 10\text{ cm}$ area inside our magnetic field.

Here it can be seen that to fully excite a $10\text{ cm} \times 10\text{ cm}$ area, we have to excite at a bandwidth of about 250 kHz . The naive solution would be to increase the bandwidth of the coils, but a broader bandwidth results in a lower Q-factor.

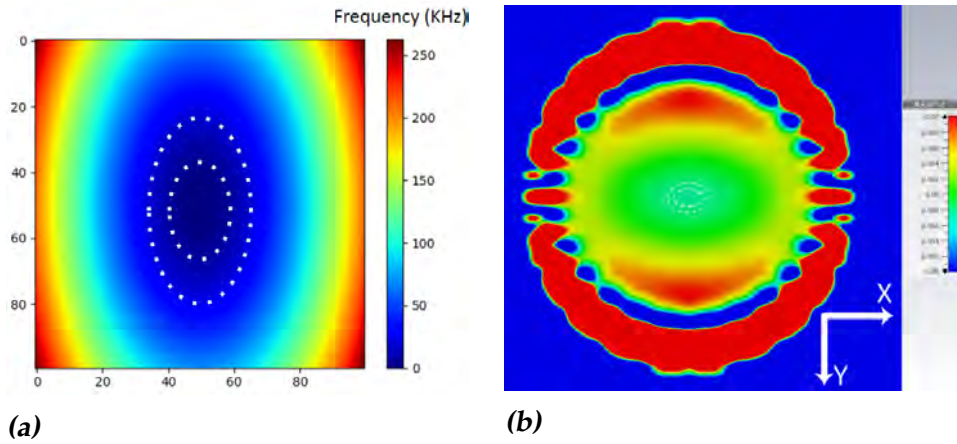


Figure 2.17: (a) shows the B_0 -map of a 10 cm x 10 cm in the middle of our magnet, the ellipses are at 20 kHz and 40 kHz bandwidth. (b) shows the size of that area compared to the whole magnet.

Simulation data provided by Thomas O'Reilly.

$$Q = \frac{\omega_R}{\text{Bandwidth}} = \frac{\omega_R L}{R} \quad (2.21)$$

Lower Q means more power is needed to obtain a signal and results in lower SNR. We want as much SNR as possible, so we want high Q , which means a narrow bandwidth and because of that less spatial coverage. This means that we need to make our magnetic field more homogeneous.

In conventional MRI systems, the magnetic field is made more homogeneous with shimming coils. These coils emit a magnetic field at the exact places where needed to further optimize the homogeneity inside the scanner. Shimming can also be done by placing permanent magnets at specific places. Another possibility regarding our set-up would be to place an end ring with magnets at the end of the bore (figure 2.18a). We are able to attach this ring to our magnet because we want to scan heads which means the magnet only has to be open at one side. The difference this end ring makes in the XY-plane is shown in figure 2.18b.

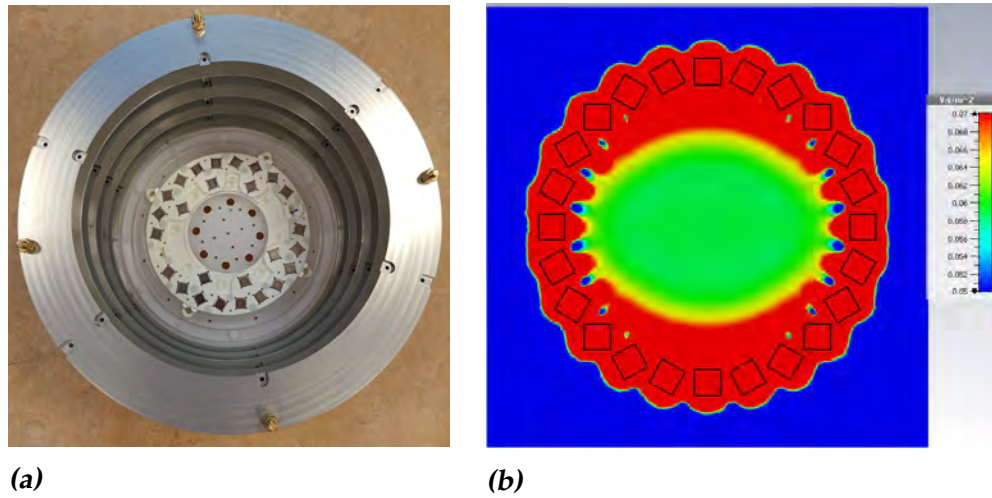


Figure 2.18: (a) shows a photo of the set-up with end ring, (b) shows the magnetic field strength inside the magnet (in the XY-plane) with the end ring attached.

2.9 Spin Echo

Instead of only the 90° -pulse used for the FID (Free Induction Decay), the spin echo sequence uses an extra 180° -pulse after a time $\frac{TE}{2}$ (Echotime). This causes the magnetization of the spins to refocus and give an echo after another $\frac{TE}{2}$ (figure 2.19).

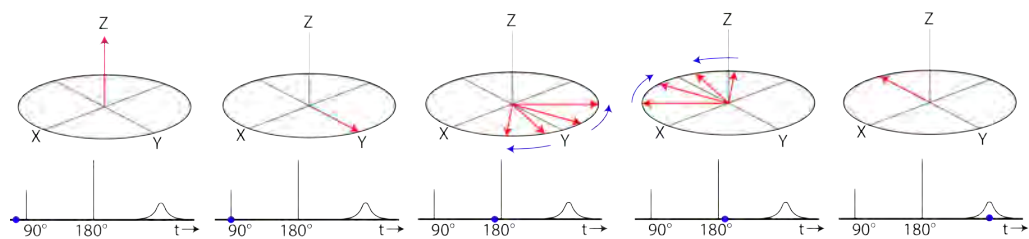


Figure 2.19: Timeline and sketch of the proton spins in the spin echo sequence.

We want to use a spin echo measurement instead of a FID because of coil ring-down. The moment the 90° degree pulse is applied, the current will still be in the coil and give a bigger signal than the MR signal our sample would give. This means that for some time after our 90° degree pulse, we cannot measure signal from our sample and the moment the coil ring-down is gone, our FID is too weak or already gone. This is why we need to use a spin echo sequence.

Chapter 3

Methodology

3.1 Coils

As explained in chapter 2.1, B_1 -fields are important for MRI. Those B_1 -fields are induced by coils in many different shapes. Figure 3.1 shows some of the coils that were already made for the Low-Field MRI. This project started with a spiral coil which was suggested to have a higher local field than previously made coils.

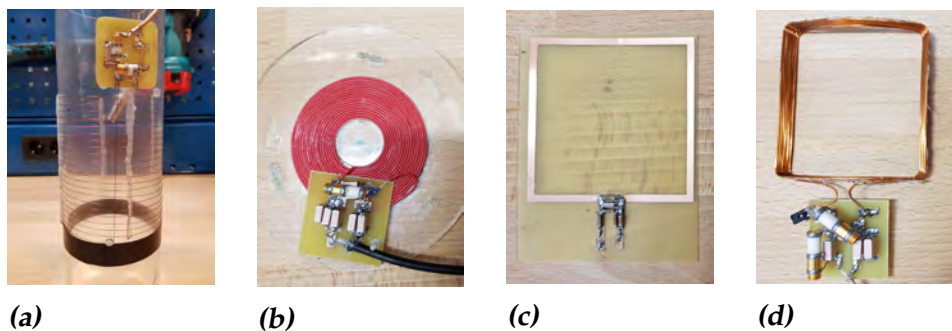


Figure 3.1: Some of the coils made for measurements. figure (a) shows a solenoid, (b) a spiral coil, (c) a surface coil with a single winding and (d) is a surface coil with 8 windings.

3.2 2D images

With a single coil and only one measurement, the only thing you obtain is a peak in the frequency spectrum. From this measurement only, we can not

directly construct a 2D image of the phantom measured. The explanation for this requires figure 2.6a. From the frequency spectrum, it is possible to use $\omega = \gamma B_0$ to find the magnetic field strength in which parts of the phantom were located. This magnetic field strength can then be used to locate the place inside the magnet where the magnetic field has the same magnitude. From this information, it is then possible to reconstruct an image. But since our magnetic field does not have an unique magnetic field strength at every place inside the magnet, our single measurement has multiple solutions for the place of the phantom (figure 2.12a).

By rotating the phantom (or the magnet around the phantom), every point inside the magnet will follow a different path of magnetic field strengths (figure 3.2). This is called rotating spatial encoding magnetic fields, rSEM for short. So by rotating the phantom, the amount of solutions gets smaller until it will eventually be 2. From rotation only, we cannot get lower than 2 since a point's mirror image will follow the exact same path in our magnetic field. This results in a reconstruction of the phantom which includes the same phantom rotated 180 degrees (figure 3.3).

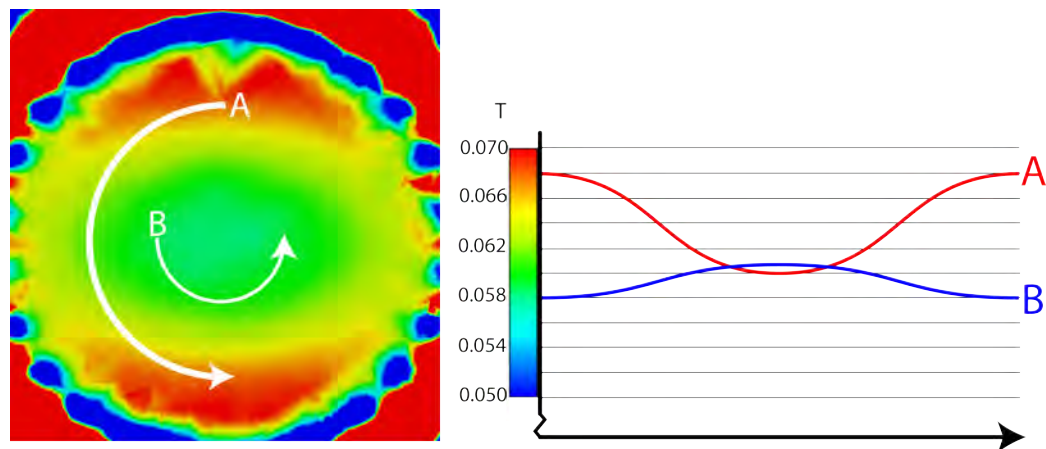


Figure 3.2: At the left the paths point A and B follow when being rotated 180 degrees, at the right the magnetic field strengths they go through during that rotation.

When combining this idea with sensitivity encoding, it is possible to reconstruct a phantom without the mirroring effect. This is the reason we constructed the 8 element RF coil array. The simulated data with this set-up and 32 rotations is shown in figure 3.4.



Figure 3.3: Reconstruction of the LUMC phantom after 32 rotations over 180 degrees with only one coil.

Simulation data provided by Thomas O'Reilly.

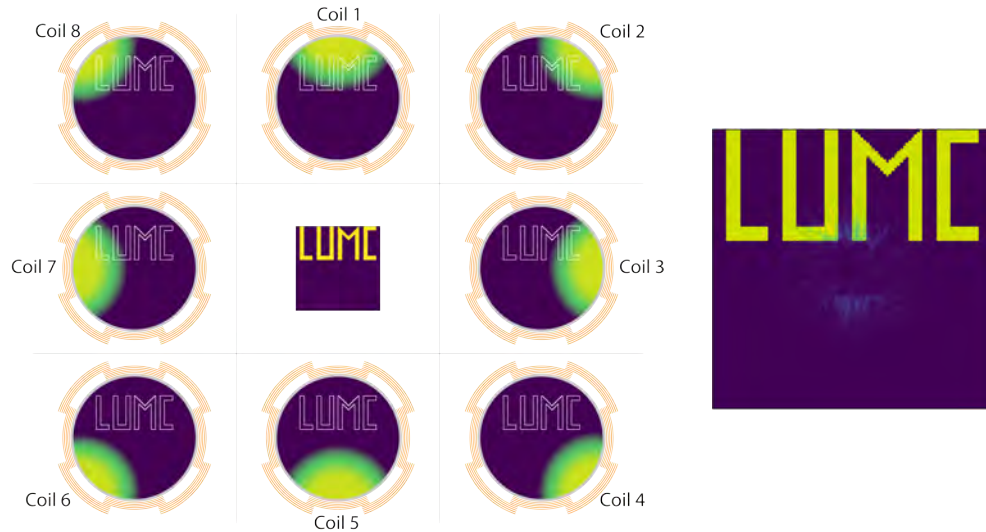


Figure 3.4: Simulation of the LUMC phantom with 8 coil sensitivity encoding and 32 rotations over 180 degrees. At the right a sketch of the coils with the sensitivity maps. Left the simulated reconstruction of the phantom.

Simulation data provided by Thomas O'Reilly.

Chapter 4

Results

4.1 First measurements

The first measurements were done with the spiral coil showed in figure 3.1b, we placed 0.5 mL oil directly on the coil and measured a spin echo (figure 4.1).

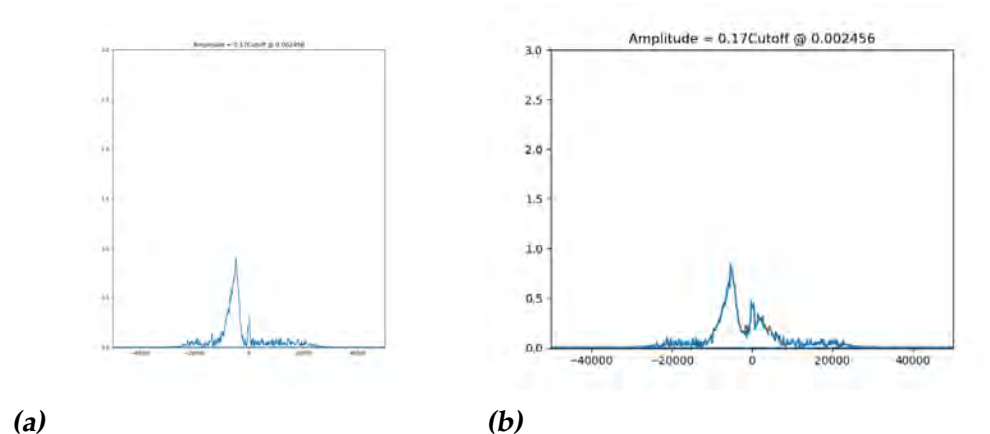


Figure 4.1: (a) Shows the frequency spectrum of the first measurement with a single phantom of 0.5 mL and (b) shows a measurement of two phantoms of 0.5 mL directly places on top of the coil.

Here it can already be seen that the measurement with the second phantom has two peaks, where the measurement of one phantom only has one clear peak. This is what one would expect because both phantoms were in another part of the magnet which means that they felt a different field strength and would thus have a different Larmor frequency.

4.2 2D images

Since it was possible to see two peaks in the frequency spectrum from two phantoms, we wanted to reconstruct a 2D images from a phantom with the spiral coil directly placed under the phantom. So we made the phantom in figure 4.2a and tried to reconstruct it after some measurements (measurement data in figure 4.3). The average total signal from these measurements was calculated with the integral under the curve of the frequency data. The parameters for these measurements are in table 4.1.

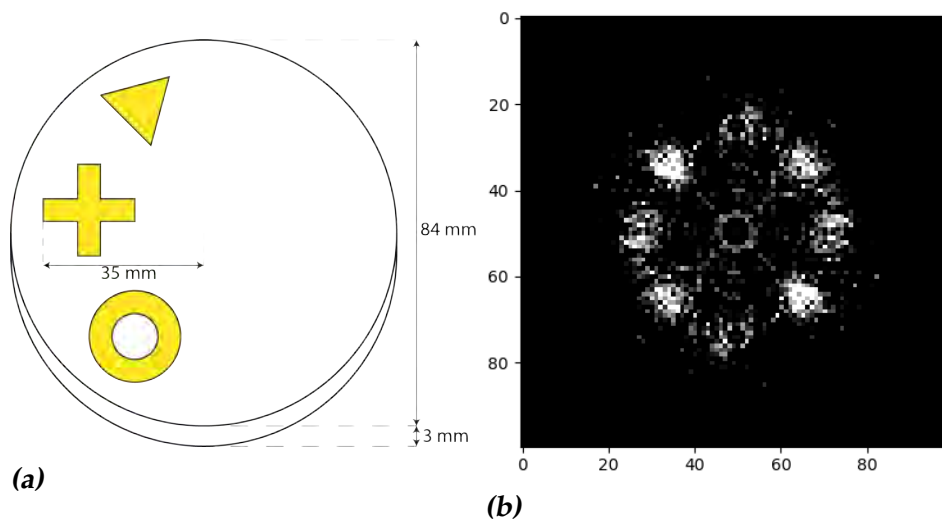


Figure 4.2: Figure (b) (scale in mm) shows the reconstruction of the phantom in (a) after 36 rotations over 180 degrees. At the left side of the picture in (a) from top to bottom a triangle, a plus and a circle. The distance from the end of the plus sign to the middle is about 35 mm.

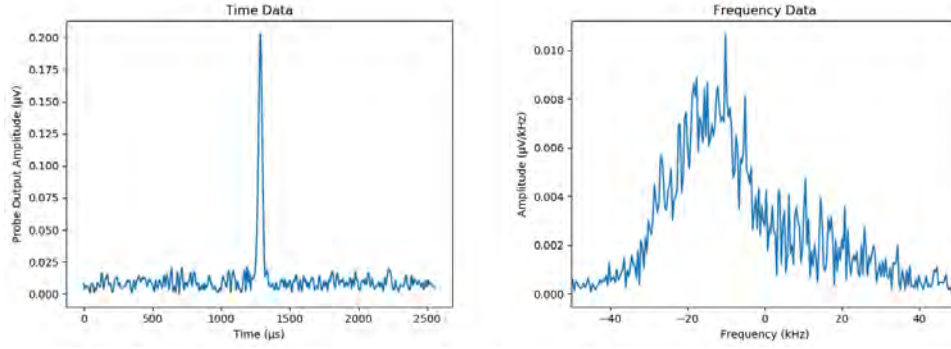
B_1 Frequency	2.56 MHz
Bandwidth Coil	75 kHz
90° / 180°Pulse	-13/ -7 dB
pulse Length	15 μ s
Echo Time	15 000 μ s
Number of Averages	250 (last 9 measurements with 500)
Dwell Time	5 μ s
Repetition Time	500 ms

Table 4.1: Parameters for the measurements in figure 4.3.

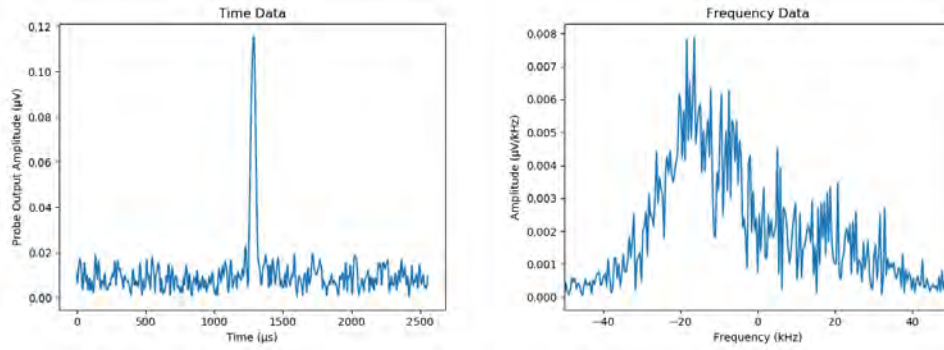
After this measurement, we started using the end ring discussed in chapter 2.8. With this new set-up, we attempted another 2D measurement with the spiral coil and the phantom from figure 4.2a. We do not have the reconstruction yet, but in this measurement (parameters in table 4.2), multiple peaks can be seen in the frequency spectrum (figure 4.4). This is exactly what you would expect from a phantom which has oil at 3 places. Next to these peaks, we also measured more signal ($2.22\mu V$ vs $0.38\mu V$ in the measurement without end ring). Also, a difference in the echo in the time data can be seen. The same method from the measurements without the end ring was used to calculate the total signal.

B_1 Frequency	2.6 MHz
Bandwidth Coil	75 kHz
$90^\circ / 180^\circ$ Pulse	-15/ -9 dB
pulse Length	25 μs
Echo Time	5 000 μs
Number of Averages	100
Dwell Time	5 μs
Repetition Time	500 ms

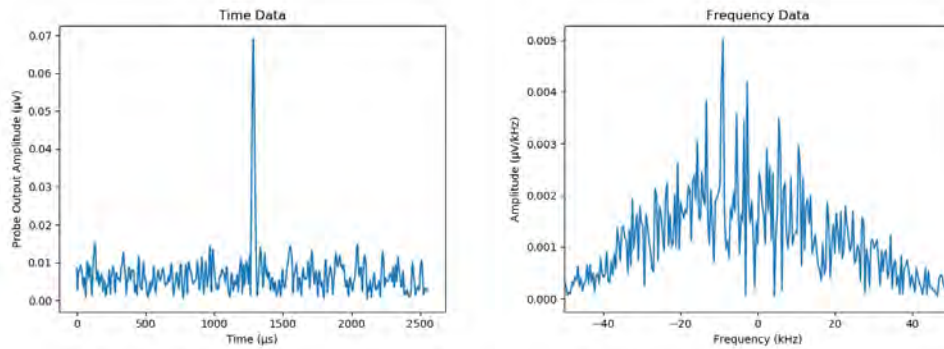
Table 4.2: Parameters for the measurements with end ring in figure 4.4.



0 Degrees

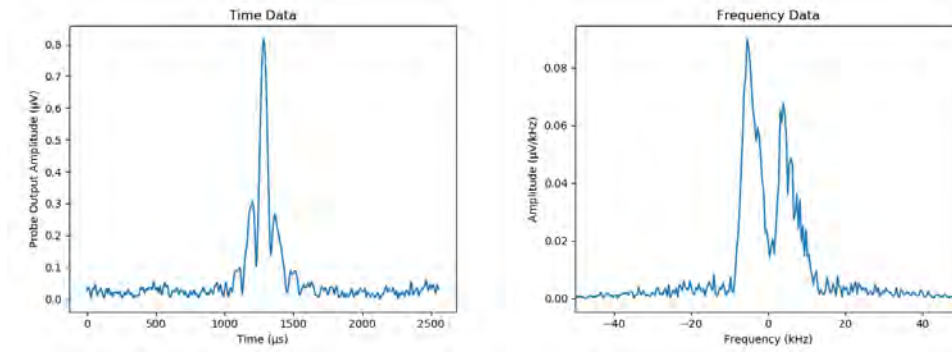


70 degrees

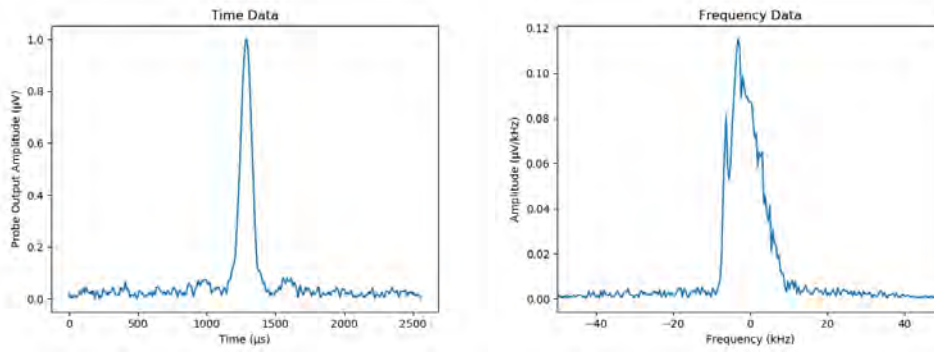


140 degrees

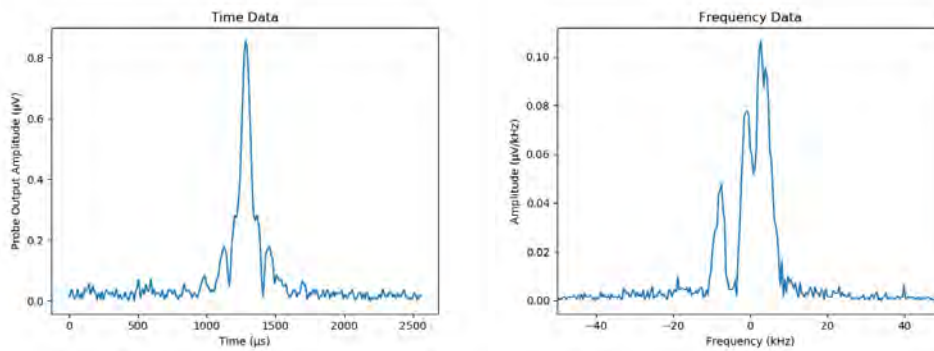
Figure 4.3: The time (left) and frequency (right) data of the measurements done for the reconstruction in figure 4.2b. This frequency data is weighted by the bandwidth of the coil: 75 kHz, the average signal is $0.38\mu V$.



0 Degrees



70 degrees



140 degrees

Figure 4.4: The time (left) and frequency (right) data of the measurements done with the phantom from figure 4.2a and with the end ring, the average signal is $2.22\mu V$.

4.3 Sensitivity Encoding

After the coils of the 8-coil array (figure 4.5 and 4.6) were tuned (table 4.3) and matched to have their resonance frequency at minimal $-40dB$, we started doing some measurements. Eventually, all coils at the same distance from the center had the same capacitor values. The first of these measurements were of a circular phantom of 120 mm diameter and 19.5 mm height, fully filled with sunflower oil. We did this measurements to optimize the flip angle for every coil (figure 4.7), these parameters were then used for every measurement with this coil array. The coils at place 1 and 5 needed less energy, since they are positioned both close to the center of the magnet and perpendicular to B_0 . The other parameters for every measurement with the coil array are shown in figure 4.8. After this optimization, we did 3 measurements of this phantom that each consisted of 200 averages to examine the difference in signal they measured. The results are in figure 4.9. After this measurement, a phantom of 50 mm diameter and 55 mm height was placed in front of one of the coils after which every coil was sequentially excited. Then the area under the frequency data curve was calculated and plotted in figure 4.10. In these graphs, no error bars are shown, the reason is that every measurement consists of 200 averages and we know that these measurements once averaged have an error smaller than 1%.

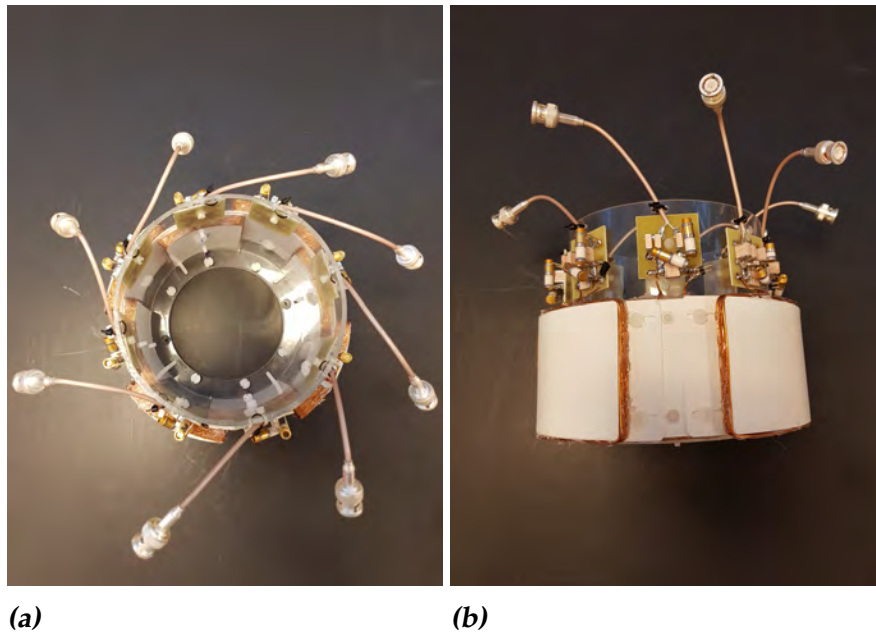


Figure 4.5: The eight coil array designed for this project.

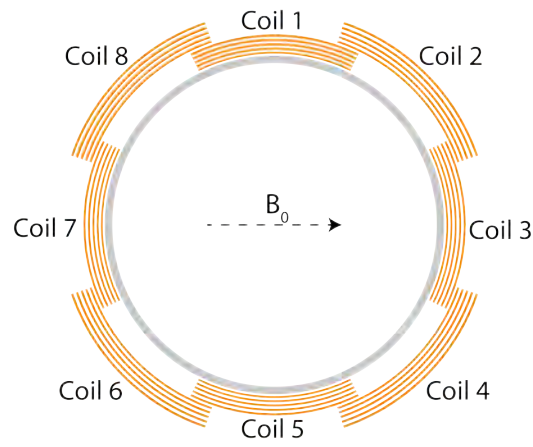


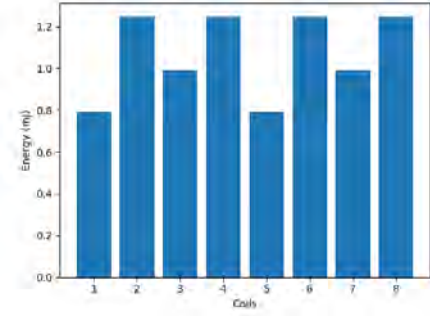
Figure 4.6: The coil set-up

Coil	B_1 frequency (MHz)	Bandwidth (kHz)
1	2.600	17.4
2	2.600	18.0
3	2.600	18.5
4	2.600	18.4
5	2.600	17.8
6	2.600	18.4
7	2.600	18.2
8	2.600	17.7

Table 4.3: The Resonance frequency and bandwidth of the coils in the coil array, the numbers correspond to the numbers in figure 4.6.

Coil	Pulse amplitude 90° / 180°(dB)	Pulse length (μs)
1	-16/ -10	50
2	-17/ -11	100
3	-18/ -12	100
4	-17/ -11	100
5	-16/ -10	50
6	-17/ -11	100
7	-18/ -12	100
8	-17/ -11	100

(a)



(b)

Figure 4.7: The optimal power requirements for every pulse depending on the coil (a) and the 'Total Energy' in (b). The 'Total Energy' used for every measurement with the eight element RF coil array, total energy is here defined as:

$$TotalEnergy(J) = \frac{(10^{\frac{90 \text{ degree pulse (dB)}}{20}} \cdot 560 \cdot 10^{-3} V)^2}{50 \Omega} \cdot 10^{\frac{50 \text{ dB}}{10}} \cdot pulselength(s)$$

We measured that 0 dB equals to 560 mV, we have 50 Ω resistance and the amplifier multiplies our signal by 50 dB.

B_1 frequency	2.6 MHz
Echo Time	5000 μs
Number of Averages	200
Dwell Time	10 μs
Repetition Time	500 ms

Figure 4.8: Parameters for every measurement done with the 8 element RF coil array.

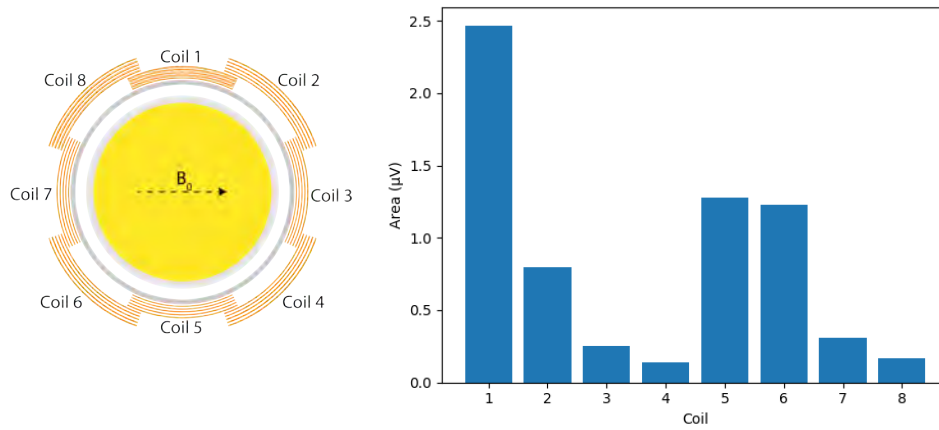


Figure 4.9: Measurements done with a phantom full of oil, 120 mm diameter and 19.5 mm height. For every coil, 3 measurements of 200 averages were done and the area under the frequency data of each measurement was averaged.

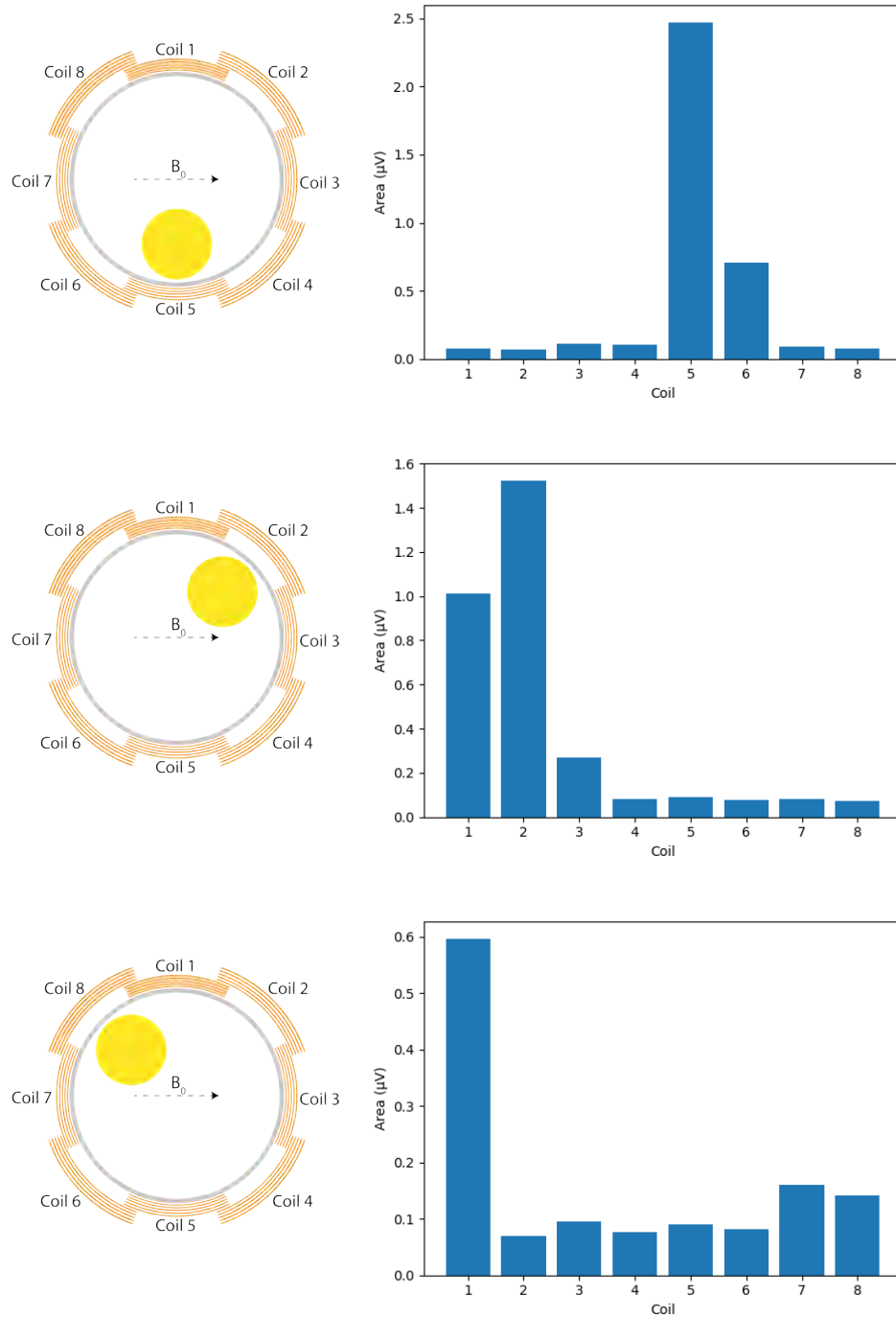


Figure 4.10: Measurements done by placing a phantom of 50 mm diameter and 55 mm height at specific places (left) and then calculated the area under the frequency curves for each of the coils (right).

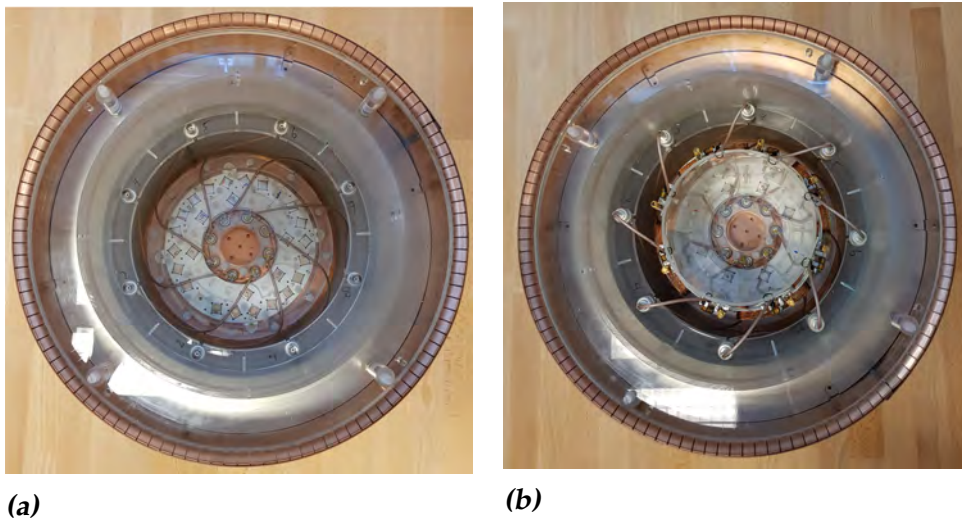


Figure 4.11: The final set-up without the coils in (a) and the set up including the coils with which the measurements from figure 4.9 and 4.10 were done in (b).

Discussion

Comparing the data of the measurements with (figure 4.4) and without (figure 4.3) end ring, it can be seen that we obtain a lot more signal (averaged: $2.22\mu V$ vs $0.38\mu V$) from the same amount of oil. An explanation for this is that the end ring provides more homogeneity in the magnetic field. Because of this, more oil can be excited by the same pulse which results in more signal. A downside of this homogeneity can be, that rSEM may become impossible because there is too little variation in field strengths for it to work.

In figure 4.9, it can be seen that not every coil measures the same amount of signal. One would expect that coil 1 and 5 receive the most amount of signal, since they are positioned perpendicular to the B_0 -field and they are (together with coil 3 and 7) closest to the sample (figure 5.1). After coil 1 and 5, the most signal is expected to come from coil 2, 4, 6 and 8. Their perpendicular component is expected to be $\cos(45^\circ)$ (with respect to B_0) times that of coil 1 and 5. The other reason one would expect their signals to be less, is because they are positioned a centimeter further away from the phantom and we expect the signal intensity to drop off with $|\vec{r}|^{-3}$. The least amount of signal is then expected from coil 3 and 7 since they are positioned along the B_0 -field.

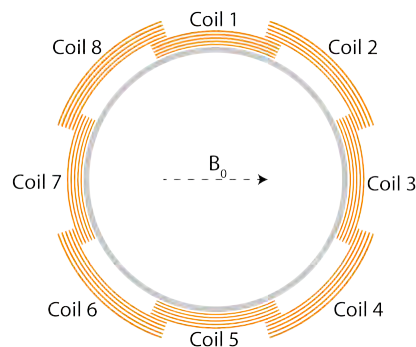


Figure 5.1: The coil set-up

But the results in figure 4.9 do not completely meet these expectations; first of all, coil 1 and 5 do not measure the same amount of signal. This can

be due to the phantom not being exactly in the middle, but also because the coils are of course hand made, which means they are not exactly the same. Next to that, coils 4 and 8 measure less signal than coils 2 and 6. They even measure less signal than coils 3 and 7,

Figure 4.10 shows that the idea of sensitivity encoding with these coils is there. When placing the phantom close to coil 5, that coil indeed measures the most amount of signal. And next to coil 5, its neighbor, coil 6, measured the most signal. It is then also expected that coil 4 would measure substantially more signal than coil 1, which is not the case. This is the reason we placed the phantom in front of coil 2, since it has two neighbors which are not coil 4 or 8. The results from this measurement are therefore promising; most signal comes from the coil the phantom was placed in front of and after that coil, its neighbors measure the most signal.

Then we were interested if coil 8 would measure the most signal when the phantom was placed in front of it, the results are shown in figure 4.10. Despite coil 8 not measuring the most signal out of all the coils as expected, it does measure more signal than with the first two measurements where the coil was not placed near coil 8.

These figures show that it may eventually be possible to use the coil array for sensitivity encoding, but before it can be achieved, some factors have to be considered. First of all, there has to be looked into coil 4 and 8 not giving the amount of signal one would expect. The other option is to place these coils at the places of coils 3 and 7, then one can ignore these coils and only use the remaining coils for measurements. Next, the angles of the coils with respect to the B_0 -field have to be considered, next to their distance from the center.

Conclusion

In this project, multiple transceive coils were made for measurements inside a Low-Field MRI system. The first coil made was a spiral coil which was eventually used for 2D measurements. We tried to reconstruct the image from it, but we did not get further than multiple spots instead of the shapes from the phantom. This measurement was later redone with an improved set up of which we do not have the reconstruction yet, but the measurement data looks more promising than that of the previous measurement.

Also, an 8-coil array was constructed. The 8 coils were needed for more signal and extra spatial encoding in 2D reconstructions. Since it was not possible to decouple these coils, they had to be sequentially excited. The first measurements for sensitivity encoding were done with these coils and showed that it may eventually be possible to use these coils for this purpose. We still have to wait for a 2D reconstruction with this coil array, because we first need to obtain sensitivity maps of these coils which will eventually be used in the reconstruction algorithm.

6.1 Acknowledgements

This project was of course not only done by me; multiple students have worked on it before me. Thomas O'Reilly was always available for questions and provided all of the knowledge needed for this project, he also provided the simulation data. Roel Burgwal also answered a lot of questions and gave tips for measurement ideas. Everyday, Lisa van Leeuwen was here to give suggestions and help with small problems. Thomas Ruytenberg and Wyger Brink were also available for suggestions from

time to time. Wouter Teeuwisse constructed the final design of the magnet shown in figure 4.11a and also helped with the construction of set ups for measurements. Thanks to prof. Andrew Webb for his input in the project and providing us with the opportunity to work on it. Also thanks to everyone from TU Delft who helped on this project; Merel de Leeuw den Bouter, Martin van Gijzen and Rob Remis for their reconstruction algorithms and input in the project, Lennart Middelpaats for designing the Magnet Array and Danny de Gans for constructing the RF-amplifier.

Bibliography

- [1] Benjamin C. Warf, Blake C. Alkire, Salman Bhai, Christopher Hughes, Steven J. Schiff, Jeffrey R. Vincent, and John G. Meara. Costs and benefits of neurosurgical intervention for infant hydrocephalus in sub-Saharan Africa. *Journal of Neurosurgery: Pediatrics*, 8(5):509–521, November 2011.
- [2] World Health Organisation. Medical equipment data by country, <http://apps.who.int/gho/data/node.main.510>.
- [3] Clarissa Zimmerman Cooley, Jason P. Stockmann, Brandon D. Armstrong, Mathieu Sarraclanie, Michael H. Lev, Matthew S. Rosen, and Lawrence L. Wald. Two-dimensional imaging in a lightweight portable MRI scanner without gradient coils: Lightweight MRI Scanner without Gradient Coils. *Magnetic Resonance in Medicine*, 73(2):872–883, February 2015.
- [4] Nadine Barrie Smith and Andrew Webb. *Introduction to Medical Imaging*. Cambridge University Press, 2011.
- [5] Klaus Halbach. Design of permanent multipole magnets with oriented rare earth cobalt material. *Nuclear instruments and methods*, 169(1):1–10, 1980.
- [6] Peter Blümli and Federico Casanova. *Hardware Developments: Halbach Magnet Arrays*. PhD thesis, University of Mainz, Mainz, 2015.
- [7] Klaas P. Pruessmann, Markus Weiger, Markus B. Scheidegger, and Peter Boesiger. SENSE: Sensitivity encoding for fast MRI. *Magnetic Resonance in Medicine*, 42(5):952–962, November 1999.

- [8] J. Haase, N. J. Curro, and C. P. Slichter. Double Resonance Probes for Close Frequencies. *Journal of Magnetic Resonance*, 135(2):273–279, December 1998.
- [9] Joël Mispelter, Mihaela Lupu, and André Briquet. *NMR Probeheads for Biophysical and Biomedical Experiments*. Imperial College Press, 2006.